www.nature.com/cdd

CDDpress

ARTICLE

The Smad4-MYO18A-PP1A complex regulates β-catenin phosphorylation and pemigatinib resistance by inhibiting PAK1 in cholangiocarcinoma

Jialiang Liu[1,8], Guangli Ren[1,2,8], Kangshuai Li[1], Zengli Liu[1], Yue Wang[1], Tianli Chen[1], Wentao Mu[1], Xiaoqing Yang[3,4,5], Xingyong Li[1,2], Anda Shi[1], Wei Zhao[1], Bowen Xu[1], Jianhua Chang[1], Sen Guo[1], Chang Pan[6], Tao Zhou[7], Zongli Zhang[1]✉ and Yunfei Xu[1]✉

Cholangiocarcinoma (CCA), consisting of three subtypes-intrahepatic (iCCA), perihilar (pCCA), and distal (dCCA), is a highly aggressive cancer arising from the bile duct and has an extremely poor prognosis. Pemigatinib is the only FDA-approved targeted drug for CCA, and the CCA treatment options are substantially insufficient considering its poor prognosis and increasing morbidity. Here, we performed next-generation sequencing (NGS) of 15 pCCAs and 16 dCCAs and detected the expression of *SMAD4*, a frequently mutated gene, in 261 CCAs. By univariate and multivariate analyses, we identified Smad4 as a favorable prognostic biomarker in iCCA and pCCA. With in vitro and in vivo experiments, we demonstrated that Smad4 suppressed CCA proliferation, migration and invasion by inhibiting β-catenin-S675 phosphorylation and intranuclear translocation. We applied LC–MS/MS and multiple biochemical techniques and identified PP1A as the phosphatase in Smad4-mediated dephosphorylation of PAK1-T423, which is responsible for β-catenin-S675 phosphorylation. Moreover, we demonstrated that MYO18A is the PP1-interacting protein of PP1A for substrate recognition in CCA. MYO18A interacts with PP1A via its RVFFR motif and interacts with Smad4 via CC domain. Patients with coexpression of MYO18A and Smad4 have a more favorable prognosis than other patients. Smad4 enhances Pemigatinib efficiency, and Smad4 knockdown results in Pemigatinib resistance. In conclusion, coexpression of Smad4 and MYO18A is a favorable prognostic indicator for iCCA and pCCA. The Smad4-MYO18A-PP1A complex dephosphorylates PAK1-T423 and thus inhibits β-catenin-S675 phosphorylation and its intranuclear localization. Smad4 suppresses CCA proliferation, migration, invasion, and sensitivity to Pemigatinib by governing the phosphorylation and intracellular localization of β-catenin.

Cell Death & Differentiation (2022) 29:818–831; https://doi.org/10.1038/s41418-021-00897-7

INTRODUCTION

Cholangiocarcinoma (CCA) is a type of highly aggressive cancer arising from the biliary system [1]. The morbidity of CCA is increasing during recent years, and East and Southeast Asia, including China, have the highest prevalence of CCA [2]. The incidence of CCA in developed countries ranged from 0.35 cases per 100,000 to 2 per 100,000 annually [3]. However, CCA incidence rises up to 85 per 100,000 in some areas in Thailand and China [4]. According to the different anatomical locations, the most contemporary classification divides CCA into three subtypes: intrahepatic (iCCA), perihilar (pCCA), and distal (dCCA) CCA [5], which have different risk factors, oncologic biology, clinical presentations, treatment methods, prognosis and epidemiological trends [1]. The prognosis of CCA is extremely poor, and the 5-year overall survival rates of different CCA subtypes after R0 resection range from 10 to 30% [6]. More unfortunately, the effects of chemotherapy and radiotherapy for CCA are very limited [7]. The only targeted drug of CCA, Pemigatinib, was approved by the FDA in 2020, but it is only effective in cases with FGFR2 fusion or mutation, which account for only 10–15% of iCCAs and <5% of pCCAs/dCCAs [8]. Overall, the shortage of CCA treatment options is substantially divergent from the poor prognosis of CCA.

Smad family member 4 (Smad4, also known as DPC4) is a central mediator of TGF-β signaling, which is a major tumor-suppressive signal in the gastrointestinal tract and pancreas [9]. Smad4 binds with Smad2/Smad3 in response to TGF-β, mediating most, but not all, TGF-β-induced signaling cascades. Smad4 is a tumor suppressor in a variety of cancers, and its genetic mutation or deletion has been reported in numerous cancer types, including pancreatic duct adenocarcinoma, colorectal cancer, CCA, gastric cancer, and prostate cancer [10–12]. The rate of *SMAD4* genetic alteration (GA) varies tremendously in different

[1]Department of General Surgery, Qilu Hospital, Cheeloo College of Medicine, Shandong University, Jinan, China. [2]Department of Hepatobiliary Surgery, Shandong Provincial Third Hospital, Cheeloo College of Medicine, Shandong University, Jinan, China. [3]Department of Pathology, The First Affiliated Hospital of Shandong First Medical University, Shandong Provincial Qianfoshan Hospital, Jinan, China. [4]Shandong Medicine and Health Key Laboratory of Clinical Pathology, Jinan, China. [5]Shandong Lung Cancer Institute, Shandong Institute of Nephrology, Jinan, China. [6]Department of Emergency, Qilu Hospital, Cheeloo College of Medicine, Shandong University, Jinan, China. [7]Department of Gastroenterology, Qilu Hospital, Cheeloo College of Medicine, Shandong University, Jinan, China. [8]These authors contributed equally: Jialiang Liu, Guangli Ren. ✉email: zzlzzl1900@163.com; xuyunfei1988@126.com

Edited by P. Salomoni

Received: 30 April 2021 Revised: 28 October 2021 Accepted: 8 November 2021
Published online: 19 November 2021

cancer types, ranging from 0.7% in glioblastoma to 55% in pancreatic duct adenocarcinoma [13, 14]. In CCA, *SMAD4* is a prevalently mutated gene according to genomic analysis [15, 16], but the clinical significance of Smad4 mutation and the correlation between Smad4 and CCA progression are still not well understood.

Smad4 has tumor-suppressive functions in multiple pathways in addition to the TGF-β signaling pathway. For example, Smad4 is reported to inhibit the activity of the WNT/β-catenin signaling pathway in cancer progression [17–19], but the molecular mechanism is not well elucidated. Existing evidence has shown that TGF-β/Smad pathways engage in crosstalk with WNT/β-catenin in the nucleus by forming a complex with β-catenin and LEF protein to synergistically regulate a set of genes [20]. In contrast, Smad4 restoration can antagonize EGF-induced phosphorylation of β-catenin [21]. The evidence showing that Smad4 enhances or suppresses WNT/β-catenin is insufficient, and many results are contradictory. In our previous study, we showed that activation of WNT/β-catenin/TCF7 signaling biasedly induced c-Myc and FOSL1 to promote the proliferation of pCCA and results in a poor prognosis [22]. Considering the importance of Wnt signaling in CCA and the significant mutation rate of Smad4, elucidating the correlation between Smad4 and WNT/β-catenin signaling in CCA is extremely critical.

In our study, we investigated the expression and prognostic significance of Smad4 in 261 patients, including 61 iCCAs, 112 pCCAs, and 88 dCCAs. Moreover, we assessed the suppressive role of Smad4 in CCA by in vitro and in vivo experiments. During this process, we found that Smad4 inhibited β-catenin-S675 phosphorylation and intranuclear translocation. With multiple experimental techniques, we identified PP1A as the key effector responsible for Smad4-involved β-catenin nuclear translocation; PP1A dephosphorylated PAK1-T423 and thus decreased β-catenin-S675 phosphorylation. Moreover, we identified MYO18A as the PP1-interacting protein (PIP) of PP1A that mediated its dephosphorylation of PAK1; it interacted with PP1A via its RVFFR motif and bind with Smad4 via its coiled coil domain. The TGF-β-independent effects of Smad4 on Pemigatinib resistance, with β-catenin as a nexus, were further evaluated by experiments in vitro and in vivo.

MATERIALS AND METHODS

CCA patients and ethics

Fifteen Chinese patients with pCCA and 16 patients with dCCA underwent surgical resection from 2017.1 to 2018.1 in Qilu Hospital of Shandong University (Supplementary Table 1). The tumor specimens were used for genetic variation detection using the next-generation sequencing (NGS)-based YuanSu™450 gene panel (OrigiMed, Shanghai, China), which covers all the coding exons of 450 cancer-associated genes and 64 selected introns in 39 genes that are frequently rearranged in solid tumors. Tumor mutational burden (TMB) was determined by measuring the somatic mutations occurring in sequenced genes including SNVs and Indels.

A total of 261 patients were obtained from 895 patients with CCA undergoing radical surgery at Qilu Hospital of Shandong University from 2012.1 to 2018.12, which were detailed as follows: iCCA (61 out of 228 cases), pCCA (112 out of 408 cases) and dCCA (88 out of 259 cases). The validation cohort was enrolled according to the following criteria: (i) patients who underwent radical resection with negative surgical margin, (ii) patients with available formalin-fixed tumor tissues, follow-up information, and complete medical records, (iii) patients with a postsurgical survival time of more than 1 month, and (iv) patients with no history of other malignancies. The tumors were classified and staged according to the 8th AJCC/UICC TNM classification system.

All the patients provided their consents for specimen obtainment and data analysis. The study protocol were approved and supervised by the Ethics Committee of Qilu Hospital of Shandong University.

Cells and agents

Human pCCA cell lines QBC-939, iCCA cell lines RBE and HCCC-9810, gallbladder cancer cell lines GBC-SD, and HCC cell lines HepG2 were obtained by the Cell Bank of Chinese Academy of Sciences (Shanghai, China). RBE, HCCC-9810 and GBC-SD were cultured in RPMI 1640 (Thermo Fisher Scientific, Waltham, MA, USA), and QBC-939 and HepG2 were cultured in DMEM (Thermo Fisher Scientific). The media for the cell lines were supplemented with 10% fetal bovine serum (Thermo Fisher Scientific), 100 U/ml penicillin, and 100 μg/ml streptomycin at 37 °C under 95% air and 5% CO_2. All cell lines were authenticated using short tandem repeat (STR) analysis, and the databases of the Chinese Academy of Sciences and American Type Culture Collection were used as references. The information of reagents and antibodies were detailed as follows:

Reagent or resource	Source	Identifier
Antibodies		
Smad4	Santa Cruz	Cat # sc-7966
β-catenin	Cell Signaling Technology	Cat # 8480
Phospho-β-catenin (ser45)	Cell Signaling Technology	Cat # 9564
Phospho-β-catenin (ser675)	Cell Signaling Technology	Cat # 4176
Phospho-β-catenin (ser552)	Cell Signaling Technology	Cat # 9566
Phospho-β-catenin (ser33/37/Thr41)	Cell Signaling Technology	Cat # 9561
PAK1	Cell Signaling Technology	Cat # 2602
Phospho-PAK1	Cell Signaling Technology	Cat # 2601
Cyclin-D1	Cell Signaling Technology	Cat # 55506
Histone H3	Immunoway	Cat # YM3038
GAPDH	Santa Cruz	Cat # sc-47724
c-Myc	Santa Cruz	Cat #sc-40
β-actin	Cell Signaling Technology	Cat # 4970
MYO18A	Proteintech	Cat # 14611-1-AP
PP1A	Santa Cruz	Cat # sc-7842
Anti-Flag M2	Cell Signaling Technology	Cat # 14793
Anti-Myc-tag	Immunoway	Cat # YM3002
PP2BB	Proteintech	Cat # 13340-1-AP
DUSP19	Proteintech	Cat # 12924-1-AP
FGFR2	Immunoway	Cat # YT0485
Mitochondria	Abcam	Cat #Ab92824
Phospho-FGFR(Y653/Y654)	R&D Systems	Cat # AF3285
Chemicals, peptides, and recombinant proteins		
Anti-Flag-tag beads	MCE	Cat #HY-K0207
Anti-c-Myc-tag beads	MCE	Cat # HY-K0206
Protein A/G beads	Santa Cruz	Cat # sc-2003
Recombinant human Wnt3a	R&D Systems	Cat #5036-WN-010
FGF-basic, human	MCE	Cat # HY-P7004
Recombinant mouse BASIC fibroblast growth factor	MCE	Cat # HY-P7066
Calyculin A	MCE	Cat # HY-18983
TGF-β	Cell Signaling Technology	Cat # 8915

IPA-3	Selleck Chemicals	Cat # 42521-82-4
SB431542	Selleck Chemicals	Cat # 301836-41-9
ICG001	Selleck Chemicals	Cat # 780757-88-2
Forskolin	Selleck Chemicals	Cat # 66575-29-9
Pemigatinib	Selleck Chemicals	Cat # 1513857-77-6
AP24534	Selleck Chemicals	Cat # 943319-70-8

Tissue microarray and IHC

Tissue microarray (TMA) was constructed using paraffin-embedded tissues as previously reported [23]. The tumor area was first identified after hematoxylin and eosin staining by a senior pathologist (XY). Core biopsies measuring 1.5 mm in diameter were taken from each sample and arranged into TMA slides.

For immunochemistry, paraffin-embedded tissue sections were deparaffinized, and antigen retrieval was achieved in 10 mmol/L sodium citrate buffer (pH 6.0). The tissue section was incubated with primary antibodies of Smad4 (1:200), FGFR2 (1:100), MYO18A (1:100), β-catenin (1:100), phospho-β-catenin-S675 (1:100) at 4 °C overnight. The appropriate secondary antibodies (Zsbio, Beijing, China) was applied for 30 min at room temperature. Subsequently, the slides were incubated with conjugated horseradish peroxidase streptavidin. The peroxidase reaction was developed using a 3,3-diaminobenzidine (DAB) solution (Zsbio).

IHC results were qualified by Quant Center software as previously reported [24], which contains the synthetical score of the staining intensity and the area of each staining. IHC score = (percentage of cells of weak intensity × 1) + (percentage of cells of moderate intensity × 2) + (percentage of cells of strong intensity × 3). The cutoff of IHC score was calculated in the receiver operating characteristic (ROC) curves [25]. The cohort was divided into subsets with low or high expression of candidate biomarkers by the cutoff.

RNA extraction and qPCR

Total RNAs of tissues and cells were extracted according to protocols using TRIzol reagent (Thermo Fisher). A reverse transcriptase kit (TOYOBO, Japan) was used to synthesize cDNA following the manufacturer's recommendations. Real-time PCR was performed using SYBR Green Master Mix (Roche, USA) and a Light Cycler Roche 480 PCR instrument. Comparison between groups was performed using the $2^{-\Delta\Delta Ct}$ method. The primers used for qPCR were listed in the following table.

qPCR primer sequence	
Smad4	F:5′ CCAATCATCCTGCTCCTGAGT 3′
	R:5′ CCAGAAGGGTCCACGTATCC 3′
β-catenin	F: 5′ GCTGCAACTAAACAGGAAGGG 3′
	R: 5′ CCCACTTGGCAGACCATCAT 3'
GAPDH	F: 5′ GAGTCAACGGATTTGGTCGT 3′
	R: 5′ GACAAGCTTCCCGTTCTCAG 3′

Western blotting

Tissue and total cell proteins were extracted using RIPA lysis buffer (Solarbio Science, Beijing, China) with 1% PMSF(Beyotime, Shanghai, China) and 1% phosphatase inhibitor (Solarbio). The nuclear and cytoplasma protein was separated using Nuclear Protein Extraction Kit (Solarbio) according to the manufacturer's instructions. After denaturation, protein samples were loaded onto 10–12% SDS-PAGE for electrophoresis and transferred to PVDF membranes (Millipore, Bedford, MA, USA). The membranes were blocked with 5% BSA and incubated with primary antibodies overnight at 4 °C and then secondary antibodies for 1 h. Protein bands were visualized using enhanced chemiluminescence (Millipore) according to the manufacturer's instructions. Quantification of the protein bands was performed using ImageJ software.

Transfection and stable cell lines

Knockdown or overexpression of Smad4 in QBC-939 and RBE cells was performed using the lentivirus (GenePharma). Other transfections of QBC-939 and RBE cells were performed using Lipofectamine 2000 (Thermo Fisher). Stable cell lines were also established with 4 μg/ml puromycin. Puromycin resistant clones were isolated for further culture. The sequences of siRNAs and shRNAs were listed in following table.

Name	The target sequence of shRNAs and siRNA (5′–3′)
shSmad4	AAGGTGGAGAGAGTGAAACAT
shPP1A	TGCTGGCCTATAAGATCAA
siPAK1-1	GCCUAGACAUUCAAGACAA
siPAK1-2	CCAAGAAAGAGCUGAUUAU
siMYO18A-1	CCCUGAGCUAGUGACUAAA
siMYO18A-2	GGCCAGUCAACUCAAAUCU
Name	**The negative sequence of shRNAs and siRNA (5′–3′)**
sh-scramble-Smad4	TTCTCCGAACGTGTCACGT
sh-scramble-PP1A	TTCTCCGAACGTGTCACGT
scrambled PAK1	CUCCGAACGUGUCACGU
scrambled MYO18A	CUCCGAACGUGUCACGU

Cell proliferation and colony formation assays

CCK-8 assays were performed to assess cell proliferation. Briefly, cells transfected with si/shRNA/overexpression sequence or corresponding scramble oligo were plated into 96-well plates (3×10^3 cells/well) and incubated for 1–4 days. Every 24 h, 10 μl of CCK-8 reagent (Dojindo, Kumamoto, Japan) was added and incubated at 37 °C for 40 min. The absorbance value at 450 nm was detected using a spectrophotometer (Molecular Devices Company).

Cells were seeded in six-well plates (1000 cells/well) and cultured with 2 mL complete medium per well at 37 °C with 5% CO_2 for 2 weeks. Medium was changed every other day, and cells were imaged. After 2 weeks, colonies were visible and washed with PBS, then fixed with methanol for 20 min, stained with 1 mg/ml crystal violet for 30 min. Colonies were counted using an microscope. At least three independent experiments were performed in triplicate.

Transwell assays

Transwell assays were performed using matrigel pre-coated 24-well plates with transwell chambers (8.0 μm 12 pore diameter; Corning). 5×10^4 RBE cells or 10×10^4 QBC-939 cells were seeded into the upper chambers with or without matrigel coated (diluted at 1:6 with RPMI 1640 or DMEM; Corning). Approximately 600 μL complete medium was added into the lower chamber. After 24–36 h of incubation, the cells attached to the bottom of chambers were fixed with methanol and stained with 0.5% crystal violet (Beyotime) for 30 min. Cell numbers were counted by ImageJ in five random visual fields of microscopy at ×200 magnification.

Immunofluorescence assay

Cells were seeded in 24-well plates on chamber slides, cultured overnight, washed with PBS and fixed with 4% Paraformaldehyde for 10 min at room temperature. After permeabilization in 0.5% Triton X-100 for 10 min, cells were incubated with 5% goat serum for 30 min at room temperature, then incubated with primary antibody (2.5% serum dilution) overnight. Secondary antibodies goat anti-mouse Alexa Fluor 488(Invitrogen,Cat#A-21202) and anti-rabbit Alexa Fluor 594 (Invitrogen,Cat #A-21207) were used to incubate cells for 1 h. Slides were mounted in Prolong Gold (Invitrogen) and stained with DAPI. Images were taken with a confocal microscopy(Carl Zeiss, LM780). The Pearson's co-localization coefficients were analyzed with Image-Pro Plus.

Renilla luciferase reporter assay

QBC-939 and RBE cells (5×10^4 cells/well) were seeded in 24-well plates in triplicate and allowed to attach for 24 h. The different preconditioning cells were then transiently transfected with the indicated plasmids and the pRL-TK Renilla luciferase plasmid using Lipofectamine 2000 (Invitrogen). 48 h after transfection, the cells were harvested and processed using a Dual-Luciferase Reporter Assay Kit (Promega, Madison, WI, USA) according to the manufacturer's instructions. Luciferase activity was evaluated using a Dual-Luciferase Reporter Assay System (Beyotime) with Renilla luciferase as internal control. TOP Flash is a luciferase reporter of β-catenin-mediated transcriptional activation with the pTA-Luc vector(Clontech). Seven TCF/LEF binding sites were cloned into the Mlu1 site of pTA-Luc vector. FOP flash is a negative control luciferase reporter with the mutated TCF/LEF sites of TOP-flash cloned into the pGL3 vector (Promega), which contains a minimal promoter followed by a firefly luciferase open reading frame. The reporter gene activity was determined by normalization of the firefly luciferase activity to Renilla luciferase activity. The TOP/FOP ratios was calculated as follows: fluorescence values of fireflies collected from samples transfected with TOP-Flash and pRL-TK Renilla luciferase plasmid(F(TOP))/fluorescence values of pRL-TK Renilla collected(R(TOP)). Fluorescence values of fireflies collected from samples transfected with FOP-Flash and pRL-TK Renilla luciferase plasmid(F(FOP))/fluorescence values of pRL-TK Renilla collected(R(FOP)).The TOP/FOP ratios was (F(Top)/R(Top))/(F(Fop)/R(Fop)).

Co-immunoprecipitation

Protein sample preparation was the same as western blotting before the addition of loading buffer. For Smad4 and PAK1/β-catenin, PAK1, and PP1A interaction, every 1 mg protein sample was incubated with 2 μg primary antibody at 4 °C overnight. Protein A/G beads (Santa Cruz Biotechnology) were added and incubated at 4 °C for 2 h. Then, sediments were collected after centrifuge at 14,000 rpm at 4 °C for 1 min and washed three times with RIPA lysis buffer. For cells expressing protein tagged with Myc or FLAG, Myc-beads or Flag beads were added into lysates and subjected to beads were mixed with loading buffer and used for western blotting detection.

LC–MS/MS analysis

QBC-939 cells were lysed using lysis buffer, and the supernatant was collected after centrifugation. Smad4 antibody was added to lysates with Protein A/G beads and incubated at 4 °C for 2 h. Protein A/G beads without Smad4 antibody incubation were set as negative control. The proteins binding with beads were washed with lysis buffer for 3 times, and denatured with 10% SDS and subjected to trypsin digestion subjected to western blotting or ingel digestion. LC–MS/MS was authorized to OEbiotech Company and performed with Orbitrap FusionTM (Thermo Scientific). Proteins found in Smad4 subgroup but not observed in negative control were defined as candidate genes interacting with Smad4.

Plasmid construction

pcDNA3.1 plasmids encoding wide type β-catenin and FLAG-MYO18A were purchased from Tsingke and GenePharma Company. S675A mutation of β-catenin and MYO18A-5A mutation were constructed through PCR-mediated site-directed mutagenesis with a QuickChangeSite-Directed Mutagenesis Kit (Agilent Stratagene, CA, USA). Different truncations of MYO18A were created by overlapping PCR in the Sequence and Ligation Independent Cloning method. The information of plasmids and primer sequences were as follows:

Plasmid	Vehicle information	Tag information
Smad4	LV5	–
β-catenin-WT	PCDNA3.1	–
β-catenin-S675A	PCDNA3.1	–
Myc-PP1A	PCDNA3.1	Myc
Flag-MYO18A-WT	PCDNA3.1	Flag
Flag-MYO18A-5A	PCDNA3.1	Flag
Flag-MYO18A-ΔPDZ	PCDNA3.1	Flag
Flag-MYO18A-ΔMD	PCDNA3.1	Flag
Flag-MYO18A-ΔMD2	PCDNA3.1	Flag
Flag-MYO18A-ΔIQ	PCDNA3.1	Flag
Flag-MYO18A-ΔCC	PCDNA3.1	Flag
Flag-MYO18A-ΔCC2	PCDNA3.1	Flag

Plasmid	Primer sequence
Flag-MYO18A-5A	F:5 GCCTGAGTGCTGCTGCTGCTGCCGCCGGCACCCTG 3′ R:5′ GTGCCGGCGGCAGCAGCAGCAGCACTCAGGCCCATGCAG 3′
Flag-MYO18A-ΔPDZ	F:5′ CACTGAGAGAGCTGAGCGAACTGAGCAGAAGCTG 3′ R:5′ CTCAGCTCTCTCAGTGTAGGAGGGGGCAGTGGCAC 3′
Flag-MYO18A-ΔMD	F:5′ CCAGCTGCAGCAGCTGCTGCATGGGCCTGAGTAGA 3′ R:5′ CAGCTGCTGCAGCTGGGGGGCGTTGGCCTTCTCCA 3′
Flag-MYO18A-ΔMD2	F:5′ CCAGCTGCGAGCAGACAAGCAGAAACCTGACACTGTTC 3′ R:5′ GTCTGCTCGCAGCTGGGGGGCGTTGGCCTTCTCCAC 3′
Flag-MYO18A-ΔIQ	F:5′ AGCAGACAATCAGATGCGTGCAGAAAAACATCAA 3′ R:5′ CATCTGATTGTCTGCTCGTCTCTCTGCTCCTCCA 3′
Flag-MYO18A-ΔCC	F:5′ TGAGCGAGGAGGGCGACAGCGACGTGGACAGCGAGCT 3′ R:5′ TCGCCCTCCTCGCTCAGCTGCACCTCGATCAGGGGTC 3′
Flag-MYO18A-ΔCC2	F:5′ TGAGCGAGTGAGGATCCACTAGTCCAGTGTGGTG-GAATTCT 3′ R:5′ GATCCTCACTCGCTCAGCTGCACCTCGATCAGGGGTC 3′

In vivo xenograft studies

Nude mice (BALB/c, female, 4–5 weeks of age, 14–16 g) were purchased from GemPharmatech Co., Ltd. (Nanjing, China) and divided randomly into groups ($n = 6$ per group). Stable Smad4-overexpressing or Smad4-silenced cells were injected subcutaneously into the right flanks to establish xenograft model (about 3×10^6 per mouse). Tumor diameter was measured every 3 day with caliper. Three to four weeks after implantation, mice were sacrificed. The final tumor volume (V) was calculated according to the following formula: $V = (L \times W^2)/2$, where L = length (mm) and W = width (mm).

For the in vivo metastasis assay, QBC-939 cells were transfected with EGFP-shSmad4 and EGFP-Smad4 by the lentivirus (GenePharma), transfected with EGFP-shPP1A using Lipofectamine 2000 (Thermo Fisher), and screened by the culture medium contained puromycin and limiting dilution in 96-well culture plates. A stable high EGFP-expressing QBC-939 cell line (Puromycin resistant clones) was obtained for further culture. The expression of EGFP of the QBC-939 cells were observed by fluorescence microscopy and selected by flow cytometry. Multiple biological behaviors, such as the growth curve and cell adherent rate were compared between the infected and uninfected cells. 4×10^5 stable high EGFP-expressing QBC-939 cells with PP1A knockdown, Smad4 knockdown or overexpression were injected into the caudal vein of each nude mouse, in the presence or absence of recombinant FGF2 (100 mg/kg i.p.) and Pemigatinib (10 mg/kg i.p.). The tumor metastases were monitored using IVIS Spectrum which can image and quantify all commonly used fluorophores, including fluorescent proteins, dyes and conjugates. The radiant efficiency was measured by Living Image Software (IVIS Imaging Systems) to quantify the tumor burden of mouse. Mouse weights were measured every week, and the weights of livers were measured to assess the actual tumor burden. The number of nodules on the livers and lungs was confirmed by H&E staining and IHC with a human mitochondria marker. All animal experiments were approved by the Medical Ethics Committee of Shandong University.

Statistical analysis

Statistical analysis were performed using SPSS17.0 (IBM, Chicago, IL, USA) and GraphPad Prism 5.0 (GraphPad Software, CA, USA). All of the western blotting films were semi-quantified with ImageJ software (National Institutes

of Health, Bethesda MD). The correlation between Smad4 and clinicopathological features was assessed by chi-sqaure test. Fisher's exact test was used to analyze the differences of frequent mutated genes in pCCA and dCCA. The correlations between the IHC score of Smad4 and the score of β-catenin in nucleus were analyzed with Pearson correlation test. Paired *t* test was used for the comparison of two paired groups. One-way or two-way ANOVA was performed to analyze the difference of multi-groups. Survival curves were plotted using the Kaplan–Meier method, and statistical significance was compared using the log-rank test. The independent prognostic factors were analyzed by multivariate analysis with Cox-regression model. *P* values < 0.05 were considered statistically significant.

RESULTS

SMAD4 is frequently mutated and aberrantly expressed in CCA

Previous studies reported that the GA of *SMAD4* ranged from 3.6 to 16.7% in iCCA [26, 27] and varied from 10.7 to 25% in extrahepatic CCA (eCCA) [28]. In our study, we performed NGS targeting 450 cancer-related genes in 15 pCCAs and 16 dCCAs. The percentages of *SMAD4* GA in pCCA and dCCA were 31.3% (5/16) and 33.3% (5/15), respectively (Fig. 1A). Interestingly, pCCA and dCCA had several other different GA rates of genes such as *ARID1A, KMT2D*, and CAMTA1; and dCCA had higher TMB (Supplementary Fig. 1). We further detected the expression of *SMAD4* in CCAs and their corresponding adjacent tissues with qPCR and WB and demonstrated that Smad4 was substantially downregulated in CCAs (Fig. 1B, C, Supplementary Fig. 2A). Immunohistochemistry (IHC) of Smad4 was performed on 61 iCCAs, 112 pCCAs, and 88 dCCAs, dividing the cohort into subsets with low or high expression of Smad4 (Fig. 1D). In the univariate survival analysis, high Smad4 was significantly associated with favorable prognoses in iCCA and pCCA (Fig. 1E), indicating that Smad4 may be a tumor suppressor in CCA. Additionally, Smad4 expression in different hepatobiliary cell lines was detected (Fig. 1F), which showed that Smad4 was expressed ubiquitously but at different levels in these cells. After Smad4 knockdown and overexpression in both RBE cells and QBC-939 cells, colony formation assay, Cell Counting Kit-8 (CCK-8) and Transwell assays showed that Smad4 overexpression suppressed CCA proliferation, migration and invasion, and Smad4 knockdown had the opposite effects (Fig. 1G–J, Supplementary Fig. 2B–D). Stable Smad4-overexpressing QBC-939 cells were injected for in vivo subcutaneous xenografts (Supplementary Fig. 2E). The xenografts with Smad4-overexpressing QBC-939 cells had decreased tumor volumes and weights compared with QBC-939 transfected with empty LV5 vector, supporting the tumor-suppressive role of Smad4 in CCA (Fig. 1K, Supplementary Fig. 2F, G).

Clinical significance of Smad4 in CCA

The correlations between Smad4 expression and other clinicopathological factors were assessed with the chi-square test. The clinicopathological factors included patient age, sex, tumor size, T stage, N stage, M stage, and tumor-node-metastasis (TNM) stage. In this clinical analysis, we demonstrated that low expression of Smad4 was significantly associated with advanced N stage in pCCA ($P = 0.004$), indicating a potential role of Smad4 in lymphatic invasion (Supplementary Table 4).

Univariate analysis was used to screen the potential prognostic factors in CCA. Interestingly, Smad4 was a favorable prognostic biomarker in iCCA and pCCA but not dCCA. In addition to Smad4, advanced T, N, M and TNM stage were also prognostic indicators for poor outcome (Supplementary Table 5). In the multivariate analysis, Smad4 was identified as an independent prognostic factor of iCCA and pCCA ($P = 0.013$ and 0.003, respectively) (Supplementary Table 6).

Smad4 inhibited the nuclear translocation of β-catenin

A previous study indicated that Smad4 suppressed tumor progression by regulating the expression of β-catenin in colon cancer [17], but we demonstrated that Smad4 expression had no significant influence on β-catenin expression in CCA cells and xenografts (Fig. 2A, B, Supplementary Fig. 3A) and that β-catenin expression in CCA tissues and adjacent tissues was not significantly different (Fig. 2C). In the mRNA sequencing of 220 iCCAs (GSE33327) and 283 eCCAs (GSE132305) [28, 29], Smad4 and β-catenin mRNA also had no significant correlation (Supplementary Fig. 3B).

Interestingly, both WB and immunofluorescence showed that β-catenin expression in the nucleus was increased by Smad4 knockdown and decreased by Smad4 overexpression (Fig. 2D, E). To verify this result, we detected the expression and location of β-catenin in CCA specimens and showed that nuclear β-catenin was negatively associated with Smad4 expression (Fig. 2F, G). Moreover, Smad4-silenced CCA cells were incubated with TGF-β or Wnt3a, while Smad4-overexpressing CCA cells were treated with the TGF signaling antagonist SB431542 or Wnt/β-catenin/TCF signaling antagonist ICG001. The results showed that Smad4-mediated β-catenin translocation was influenced by Wnt signaling but not TGF signaling (Fig. 2H). TOP/FOP-Flash luciferase assays were conducted to detect the activation of genes downstream of β-catenin. The results showed that intranuclear β-catenin enhanced transcriptional activity under Wnt signaling stimulation, and that high SMAD4 expression cannot modify Wnt signaling if β-catenin was inhibited (Fig. 2I, J).

S675 phosphorylation by PAK1 was essential for β-catenin nuclear translocation

The phosphorylation patterns of β-catenin-mediated different cellular processes, so we screened different β-catenin phosphorylation sites and found that S675 phosphorylation was substantially decreased after Smad4 overexpression (Fig. 3A). Previous studies reported that PAK1 was a potential kinase phosphorylating β-catenin-S675 [30], and indicated an interaction between PAK1 and Smad4 with a high-throughput method [31]. Here, we immunoprecipitated Smad4 in RBE cells and consequently demonstrated that both β-catenin and PAK1 interacted with Smad4 in RBE cells (Fig. 3B). The immunofluorescence also showed a co-localization of Smad4 and PAK1 after Wnt3a stimulation (Supplementary Fig. 4A). Furthermore, Smad4 expression did not regulate PAK1 expression (Supplementary Fig. 4B), but inhibited the phosphorylation of PAK1-T423 and β-catenin-S675 in both RBE and QBC-939 cells (Fig. 3C). Wnt3a stimulation enhanced the phosphorylation of both PAK1-T423 and β-catenin-S675 in QBC-939 cells (Supplementary Fig. 5). Furthermore, we knocked down PAK1 or inhibited PAK1 activity via IPA-3, and showed that β-catenin-S675 phosphorylation was the subsequent result of PAK1 phosphorylation (Fig. 3D, E). To further validate the role of PAK1 in Smad4-mediated β-catenin phosphorylation, we silenced PAK1 expression or inhibited PAK1 activation in Smad4-silenced RBE cells. PAK1 knockdown or activity suppression inhibited β-catenin phosphorylation, which was induced by Smad4 knockdown (Fig. 3F). In contrast, the PAK1 stimulator forskolin eliminated the inhibitory effect of Smad4 on β-catenin phosphorylation (Fig. 3G). These results showed that PAK1 was the key effector in Smad4-mediated β-catenin phosphorylation. With WB and immunofluorescence assays, we showed that PAK1 induced the intranuclear translocation of β-catenin in RBE and QBC-939 cells, which was suppressed by Smad4 (Fig. 3H, I, Supplementary Fig. 6).

Furthermore, we transfected Smad4-silenced CCA cells with plasmids encoding wild-type or S675A-mutant β-catenin. β-catenin overexpression increased the transcription and expression of genes downstream Wnt/β-catenin signaling such as c-Myc and cyclin-D1 (Supplementary Fig. 7). Overexpression of wild-type β-catenin promoted the proliferation, migration and invasion of Smad4-silenced CCA cells, whereas β-catenin-S675A had the opposite effects (Fig. 3J, L, Supplementary Fig. 8A, B). In vivo experiments also showed that Smad4 knockdown and β-catenin

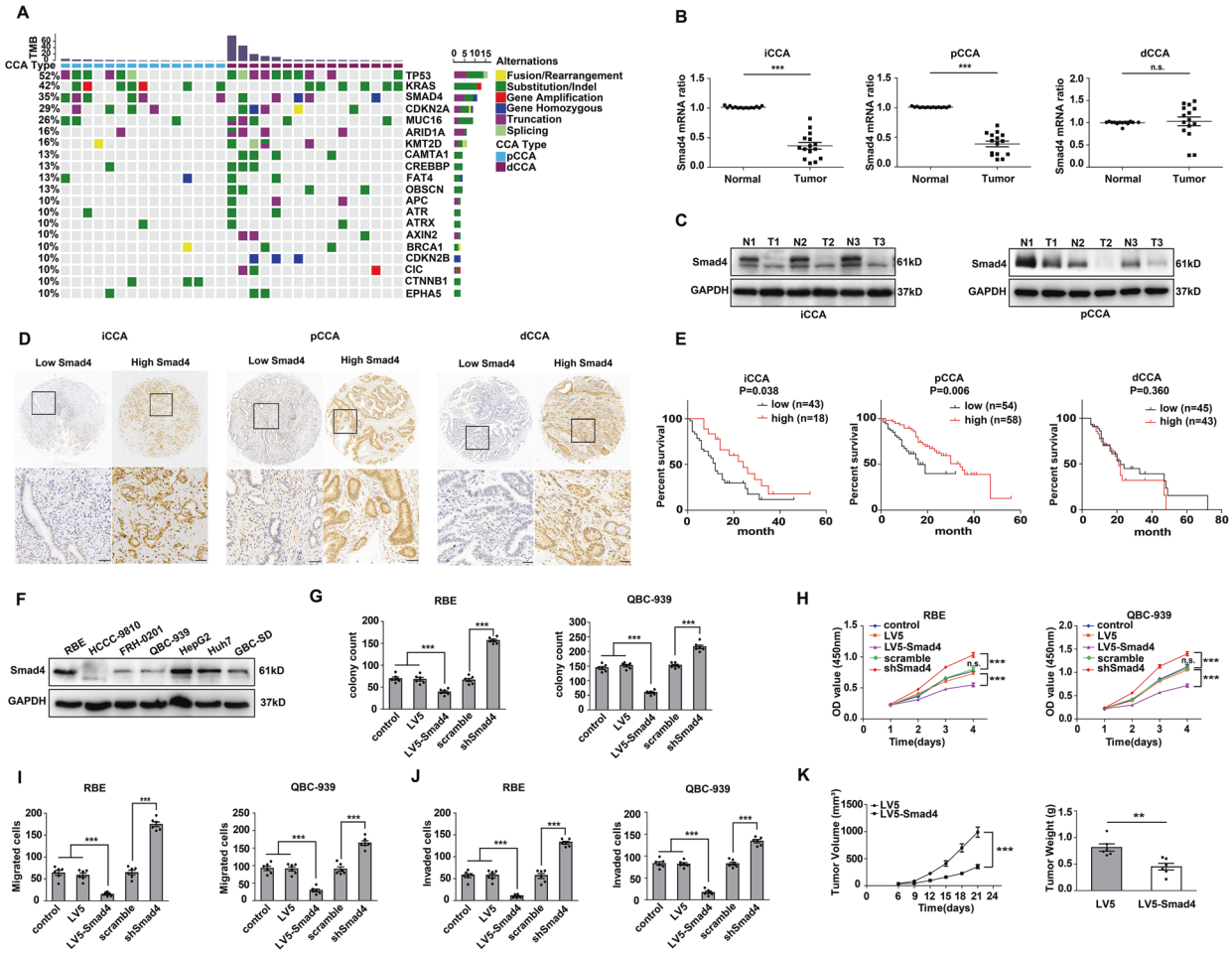

Fig. 1 The genomic alteration, expression and function of Smad4 in CCA. A Frequency of genomic alterations in 15 pCCAs and 16 dCCAs. **B**, **C** The expression of Smad4 was detected with qPCR in 15 pairs of CCAs and adjacent tissues (**B**), and with WB in three pairs of CCAs and adjacent tissues (**C**). **D** Smad4 expression was detected by IHC, and patients with CCA were divided into subsets with low and high Smad4 expression. Scale bar: 50 μm. **E** The correlation between Smad4 expression and overall survival in CCA was calculated with the log-rank test. **F** Smad4 expressions in different hepatobiliary tumor cell lines: iCCA cell lines RBE and HCCC-9810, pCCA cell lines QBC-939, and FRH-0201, hepatocellular carcinoma cell lines HepG2 and Huh7, gallbladder carcinoma cell line GBC-SD. **G**–**J** Smad4 inhibited the proliferation, migration and invasion of iCCA and pCCA cell lines. Cell proliferation was evaluated with colony formation assay (**G**) and CCK-8 assay (**H**). Cell migration (**I**) and invasion (**J**) were investigated with Transwell assays. **K** Xenografts were established with stable Smad4-silenced QBC-939 cells. Mice engrafted with Smad4-overexpressing cells less tumor volumes (left) and tumor weights (right). $^{**}P < 0.01$, $^{***}P < 0.001$ analyzed by paired *t* test (**B**), log-rank test (**E**), one-way ANOVA (**G**, **I**, **J**), or two-way ANOVA (**H**, left panel of **K**). Data were from at least three independent experiments (**B**, **C**, **F**–**J**) and shown as the mean ± S.E.M.

overexpression increased tumor volume and weight; however, β-catenin-S675A overexpression decreased xenograft volume and weight (Fig. 3M, Supplementary Fig. 8C). These results suggested that phosphorylation of β-catenin was a key effector in the CCA-suppressing role of Smad4 and that S675A was a dominant-negative mutation in Smad4-mediated CCA progression.

PP1A interacted with Smad4 and dephosphorylated PAK1 at the T423 site

To identify the key factor responsible for Smad4-mediated PAK1 dephosphorylation, we immunoprecipitated Smad4 from QBC-939 cells and performed LC–MS/MS to screen the proteins interacting with Smad4. Three serine/threonine phosphatases were discovered, including PP1A, PP2BB and DUSP19 (Fig. 4A) (Supplementary Table 7). Immunoprecipitation of PAK1 in QBC-939 cells further indicated that PAK1 interacted with PP1A instead of PP2B or DUSP19 (Fig. 4B). Therefore, we further inhibited PP1A activation by calyculin A or regulated PP1A expression by overexpressing or knocking down PP1A in CCA cells. Calyculin A and PP1A knockdown significantly promoted PAK1-T423 phosphorylation and subsequent β-catenin-S675A phosphorylation, while PP1A overexpression had the opposite effects (Fig. 4C, D). Moreover, a plasmid encoding Myc-tagged PP1A was transfected into RBE cells, and calyculin A was shown to inhibit the PP1A–PAK1 interaction with co-immunoprecipitation (Fig. 4E). With co-immunoprecipitation and immunofluorescence, we proved that the interaction between PAK1 and PP1A was facilitated by Smad4 overexpression and disrupted by Smad4 knockdown (Fig. 4F, H). Moreover, CCK-8 and Transwell assays suggested that PP1A suppressed the proliferation, migration and invasion of CCA cells (Fig. 4I, L, Supplementary Fig. 9). The above results suggested that PP1A dephosphorylated phospho-PAK1-T423 and inhibited CCA progression in a Smad4-dependent manner.

MYO18A was the PIP mediating PP1A catalysis towards PAK1

The PP1 family requires PIP participation for substrate recognition and intracellular localization [32]. Most PIPs have a consensus sequence "RVFFR" to bind PP1, but Smad4 has no similar motif. We

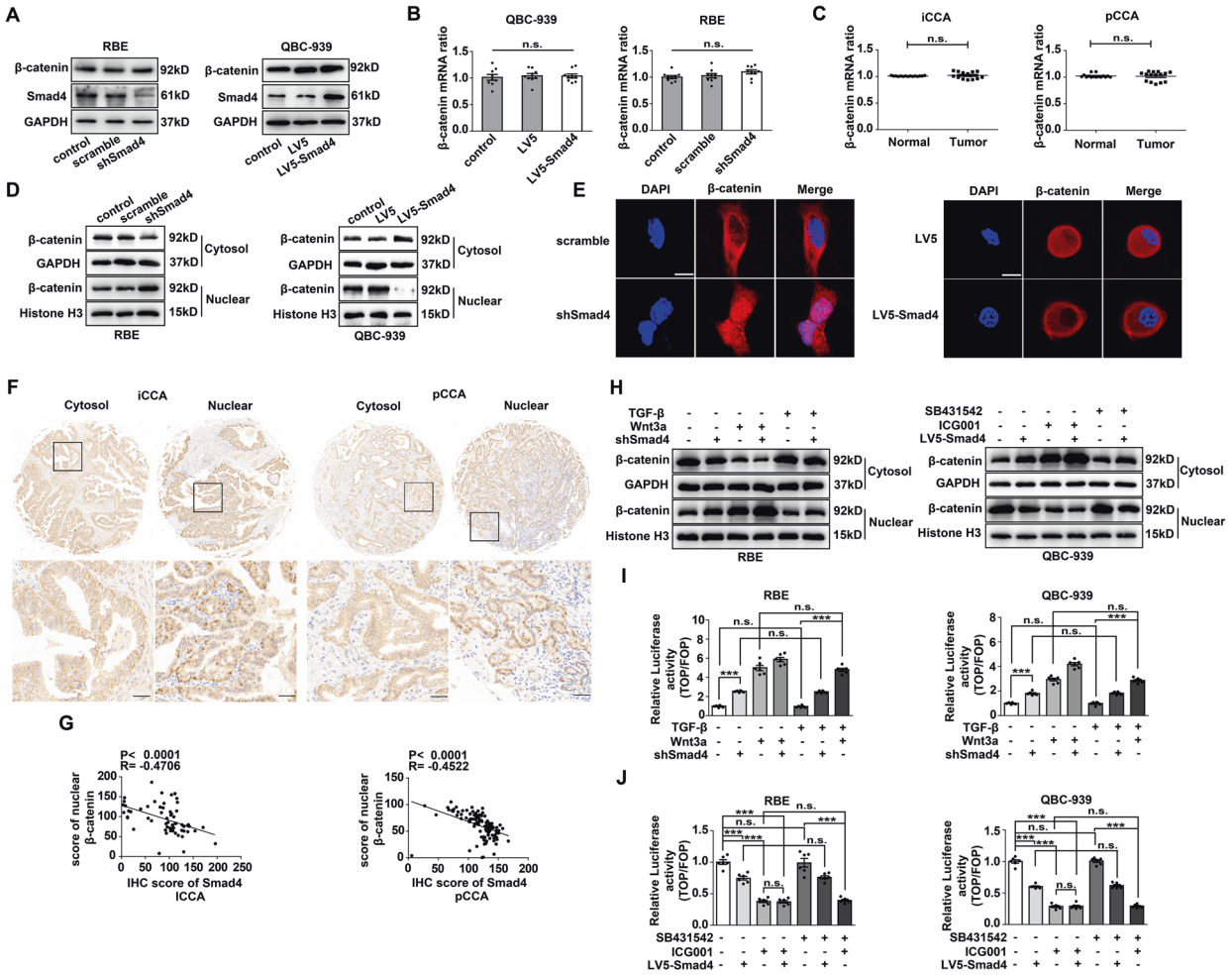

Fig. 2 Smad4 expression was associated with the intracellular location of β-catenin. WB (**A**) and qPCR (**B**) showed that Smad4 expression did not regulate the expression of β-catenin in QBC-939 and RBE cells. qPCR showed that β-catenin expression was not significantly different in CCAs and adjacent tissues. **D**, **E** Smad4 expression was silenced in RBE cells or overexpressed in QBC-939 cells. β-catenin expression in the nucleus and cytosol was detected by WB (**D**) and immunofluorescence (**E**). **F** β-Catenin expression was detected by IHC in CCA specimens. Representative images of the cytosol and nuclear expression of β-catenin are shown. **G** The IHC scores of Smad4 were negatively correlated with the β-catenin score in the nucleus. **H** After treatment with Wnt3a (100 ng/mL) or TGF-β (5 ng/mL) in RBE cells or with ICG-001 (10 μM) or SB431542 (10 μM) in QBC-939 cells for 12 h, β-catenin expression in the nucleus and cytosol was detected. **I**, **J** TOP/FOP-Flash activity was detected to assess the transcriptional activity of β-catenin. After transfection with TOP/FOP/TK plasmids, RBE, and QBC-939 cells were treated with Wnt3a (100 ng/mL) or TGF-β (5 ng/mL)(I), ICG-001 (10 μM) or SB431542 (10 μM)(J) for 24 h. n.s. not significant; $^{**}P < 0.01$; $^{***}P < 0.001$. Data were from three independent experiments and analyzed by log-rank test (**B**), paired *t* test (**C**), one-way ANOVA (**A**, **I**, **J**), or Pearson's correlation test (**G**). Mean ± S.E.M. (error bar) was used to show the data.

screened the sequences of proteins in LC–MS/MS, only MYO18A had an RVFFR motif from site 1169 to site 1173. By further sequence alignment, this RVFFR sequence is unique in MYO18A and highly conserved in different MYO18A species (Fig. 5A), implying that this sequence may be pivotal in some special functions of MYO18A. Additionally, we silenced MYO18A in CCA cells and showed that MYO18A knockdown not only increased PAK1-T423 phosphorylation but also impaired the interaction between PP1A and PAK1 (Fig. 5B, C). This result suggested an essential role of MYO18A in the catalysis of PP1A to PAK1. Furthermore, we designed several truncation constructs of MYO18A to identify the key motif responsible for the PP1A and PAK1 interaction (Fig. 5D). MYO18A-5A (RVFFR mutated to AAAAA) and ΔMD-2 (405–1085 deletion) mutations significantly decreased the interaction between MYO18A and PP1A. However, the MYO18A-ΔMD mutation (405–1160 deletion) had no substantial influence on the MYO19A-PP1A interaction because the MYO18A-ΔMD mutation contained the RVFFR motif (Fig. 5E). MYO18A overexpression decreased the phosphorylation of PAK1-T423 and downstream β-catenin-S675, but MYO18A-5A overexpression had no similar effect (Fig. 5F). The above results showed that MYO18A was a PIP mediating PP1A catalysis towards phospho-PAK1-T423. More interestingly, we accidently found that the MYO18A-ΔCC mutation had no significant effect on the MYO18A-PP1A interaction but impaired the interaction between MYO18A and PAK1. Therefore, we investigated the function of the CC domain and showed that the CC domain was responsible for the MYO18A interaction with Smad4 (Fig. 5G). Under Wnt3a stimulation, MYO18A co-localized more with PP1A and Smad4 (Supplementary Fig. 10A, B). However, the MYO18A-5A mutation decreased the co-localization with PP1A, and the MYO18A-ΔCC mutation impaired the co-localization of MYO18A with Smad4 (Supplementary Fig. 10C, D). These results indicated that MYO18A interacted with PP1A by the RVFFR motif and with Smad4 by the CC domain in CCA cells.

Moreover, we silenced or overexpressed MYO18A in CCA cells and showed that MYO18A knockdown significantly enhanced CCA proliferation, migration and invasion (Fig. 5H, Supplementary

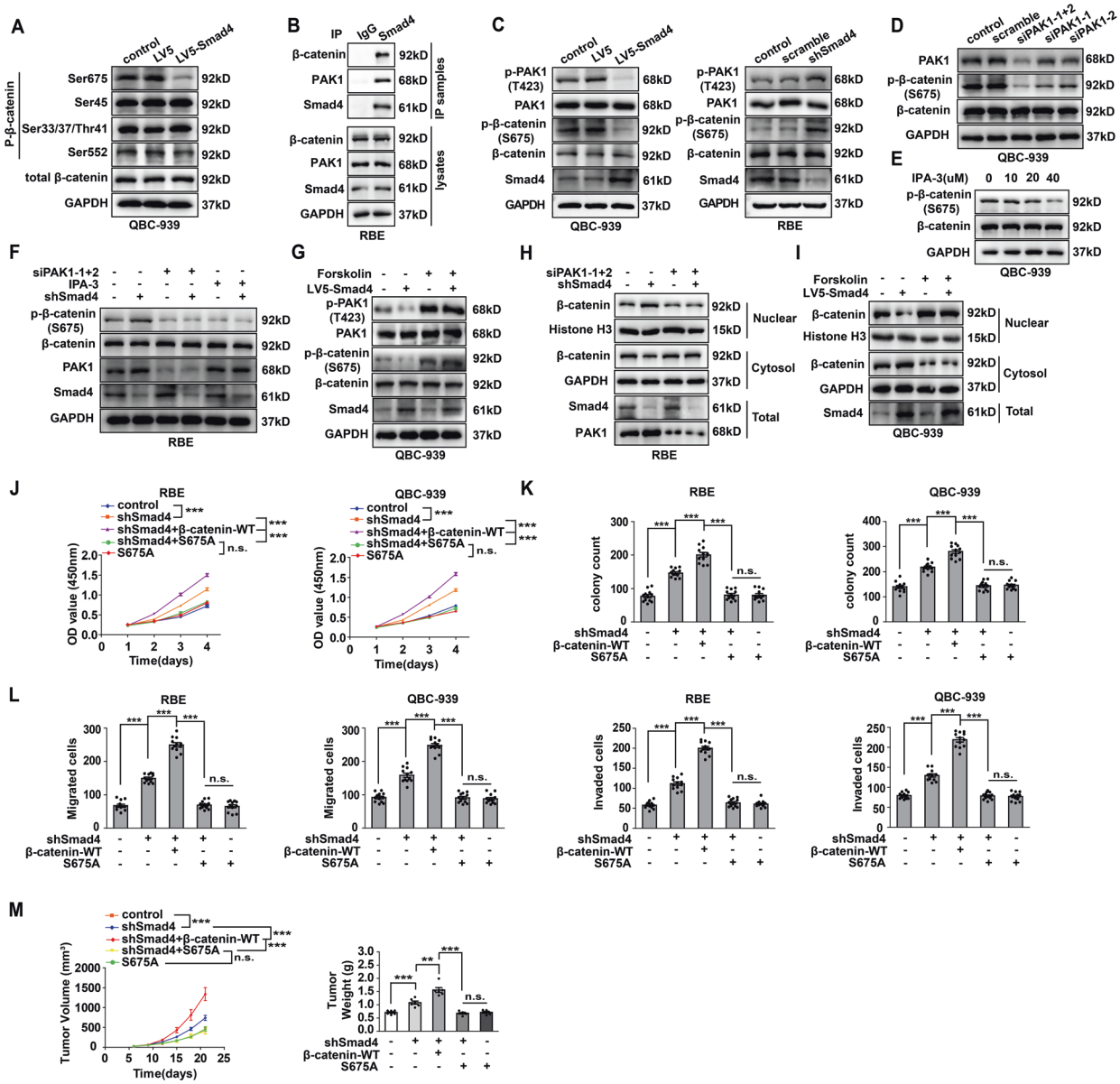

Fig. 3 Smad4 mediated the PAK1-induced S675 phosphorylation of β-catenin. A Phosphorylation of different tyrosine sites of β-catenin after Smad4 overexpression. **B** Smad4 interacted with PAK1 and β-catenin in CCA. Primary antibody against Smad4 was used for immunoprecipitation of RBE cells. PAK1 and β-catenin in the output were detected by WB. **C** After overexpressing Smad4 in QBC-939 cells (left) or silencing Smad4 in RBE cells (right), the phosphorylation of PAK1-T423 and β-catenin-S675 was detected. β-catenin-S675 phosphorylation was detected after decreasing PAK1 expression (**D**) or inhibiting PAK1 (**E**). **F** In Smad4-silenced RBE cells, PAK1 was knocked down or inhibited by IPA-3, and β-catenin-S675 phosphorylation in total lysate was detected with WB. **G** In Smad4-overexpressing QBC-939 cells, PAK1 was stimulated with forskolin (20 μM) for 12 h (right), and β-catenin-S675 phosphorylation in total lysate was detected with WB. PAK1 was knocked down in Smad4-silenced RBE cells (**H**), or stimulated with forskolin in Smad4-overexpressing QBC-939 cells (**I**), proteins in nuclear and cytosol were separated to detect β-catenin intracellular localization. CCK-8 assay (**J**), colony formation assay (**K**) and transwell assay (**L**) showed that S675A mutation of β-catenin inhibited the proliferation, migration, and invasion of CCA cells. **M** Subcutaneous xenografts in nude mice were established with stable Smad4-silenced QBC-939 cells overexpressing wild-type or S675A-mutant β-catenin. The tumor volume (top) and weight (bottom) of subcutaneous xenografts were measured. In (**J**–**M**), ** represents $P < 0.01$, *** represents $P < 0.001$, with one-way or two-way ANOVA. The experiments were conducted in triplicate, and the analyzed data are displayed as the mean ± S.E.M.

Fig. 11). MYO18A overexpression attenuated CCA progression, but MYO18A-5A overexpression had no such effects, suggesting that the RVFFR motif was essential in the tumor-suppressing role of MYO18A (Fig. 5I, Supplementary Fig. 11). MYO18A expression in CCA was further investigated with IHC, dividing the cohort into subsets with low and high MYO18A expression (Fig. 5J). MYO18A expression itself had no significant prognostic significance (Supplementary Fig. 12A), but further stratification combining both Smad4 and MYO18A had higher sensitivity for prognosis than Smad4 alone (Fig. 5K). Patients with high expression of both Smad4 and MYO18A usually had more favorable outcomes than those with only Smad4 expression. Interestingly, MYO18A expression in CCA tissues was negatively associated with the phosphorylation of β-catenin-S675 (Supplementary Fig. 12B, C), which validated our in vitro results in clinical specimens.

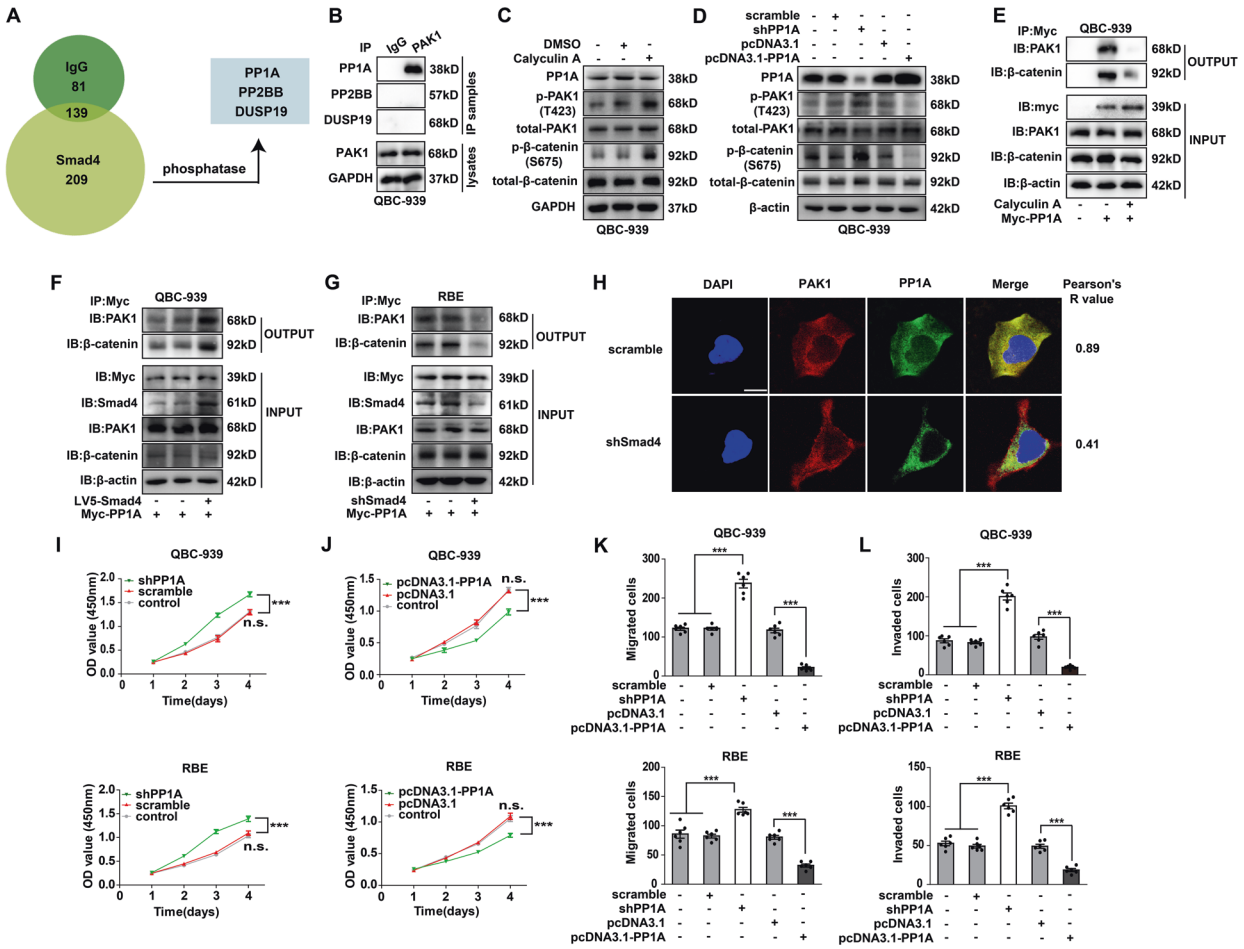

Fig. 4 PP1A was the key phosphatase involved in Smad4-mediated PAK1 phosphorylation. A LC–MS/MS was applied to screen out three phosphatases interacting with Smad4 in QBC-939 cells. **B** Immunoprecipitation with PAK1 primary antibody showed the interaction between PAK1 and PP1A in RBE cells. PP1A activity was inhibited by calyculin A (2 nM) treatment for 12 h (**C**), or PP1A was knocked down or overexpressed in QBC-939 cells (**D**). Phosphorylation of PAK1-T423 and β-catenin-S675 was detected. **E** QBC-939 cells were transfected with Myc-PP1A and incubated in calyculin A. Myc antibody was used for immunoprecipitation, and precipitated PAK1 in output was detected with WB. **F**, **G** Smad4-overexpressing QBC-939 or Smad4-silenced RBE cells were transfected with Myc-PP1A. Myc antibody was applied for immunoprecipitation, and PAK1 expression in the output was detected. **H** The expression and localization of PAK1 and PP1A in RBE cells were detected with immunofluorescence. The co-localization of PAK1 and PP1A was attenuated after Smad4 knockdown. Scale bar 10 μm. PP1A was silenced (**I**) or overexpressed (**J**) in RBE and QBC-939 cells, and proliferation was detected with CCK-8 assay. Migration (**K**) and invasion (**L**) were detected with PP1A-overexpressing and PP1A-silenced CCA cells. n.s. represents not significant, and *** represents $P < 0.001$, analyzed with one-way or two-way ANOVA. Data were analyzed in triplicate (**B**–**L**) and shown as the mean ± S.E.M.

Smad4 suppressed FGFR2-induced progression in CCA by inhibiting β-catenin phosphorylation

FGFR2 is a well-accepted oncoprotein of CCA, and its inhibitor Pemigatinib is the only FDA-approved targeted drug for CCA [8]. A previous study indicated potential crosstalk between FGFR2 and Wnt signaling [33], so we further investigated the role of Smad4 in FGFR2-induced CCA progression. First, Smad4-overexpressing CCA cells were treated with Pemigatinib or another pan-FGFR inhibitor AP24534 (Fig. 6A, B). In CCA cells, FGF2 significantly increased phosphorylation of β-catenin-S675, whereas Pemigatinib and AP24534 substantially inhibited this FGF2-induced phosphorylation. Smad4 overexpression had an analogous suppressive effect on FGF2-induced β-catenin-S675 phosphorylation like Pemigatinib. Moreover, Smad4 overexpression inhibited FGF2-induced CCA proliferation, migration and invasion and increased the Pemigatinib-induced inhibition of CCA progression (Fig. 6C–E). Smad4 knockdown attenuated the inhibitory effect of Pemigatinib on CCA progression, while β-catenin-S675A and the PAK1 inhibitor IPA-3 attenuated FGF2-induced CCA progression (Fig. 6F, G). In the mice metastatic model, we also showed that Smad4 knockdown substantially counteracted the inhibitory effect of Pemigtinib on CCA metastasis (Fig. 6H, I). With in vitro experiments and an in vivo metastatic model, we also showed that FGF2-induced CCA proliferation, migration and invasion were enhanced by Smad4 knockdown and suppressed by Smad4 overexpression (Supplementary Fig. 13A–F). PP1A knockdown also abrogated the suppressive function of Smad4 on CCA progression (Fig. 6J–M). In clinical specimens, the correlations between β-catenin-S675 phosphorylation, Smad4 and FGFR2 were analyzed. Consistent with the biochemical data, Smad4 expression was negatively correlated with β-catenin-S675 phosphorylation, and FGFR2 expression was potently associated with β-catenin-S675 phosphorylation (Fig. 6N, O). Taken together, the results showed that Smad4 antagonized FGF2-induced β-catenin-S675 phosphorylation in CCA cells. Smad4 expression level influenced Pamigatinib sensitivity and Smad4 knockdown conferred CCA cells resistance to Pamigatinib.

DISCUSSION

CCA was previously classified as iCCA and extracellular CCA (eCCA) until the 7th American Joint Committee on Cancer (AJCC)/Union

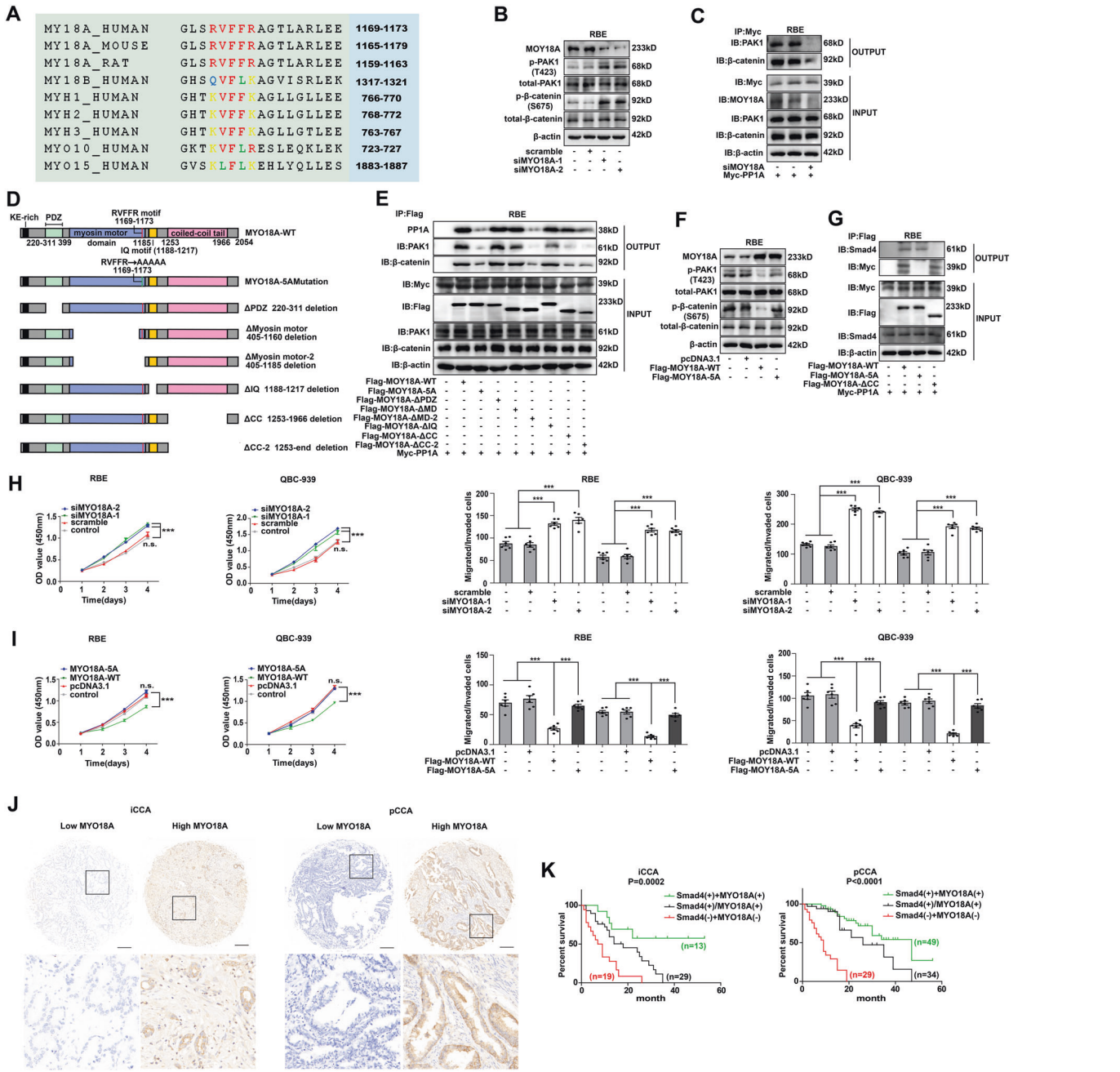

Fig. 5 Myosin 18A mediated the PP1A–PAK1 interaction via the RVFFR motif. A The consensus sequence alignment of Myosin family proteins. **B** After MYO18A knockdown in RBE cells, the phosphorylation of PAK1-T423 and β-catenin-S675 was detected, **C** PAK1 was detected in the Myc-immunoprecipitated output after Myc-PP1A overexpression. **D** The schematic depicts different truncations of MYO18A. **E** PP1A-overexpressing RBE cells were transfected with plasmids encoding different FLAG-MYO18A mutations. FLAG beads were used for immunoprecipitation, and Flag-immunoprecipitated PP1A and PAK1 were detected in the output by WB. **F** RBE cells were transfected with MYO18A-WT or MYO18A-5A mutation, and the phosphorylation of PAK1 and β-catenin was detected. **G** Plasmids encoding Flag-MYO18A-WT, −5A or −ΔCC were transfected into PP1A-overexpressing RBE cells, and Flag-immunoprecipitated Smad4 in the output was detected. QBC-939 and RBE cells were transfected with siMYO18A (**H**) or plasmids encoding MYO18A-WT/5A mutation (**I**). Proliferation, migration, and invasion were detected with CCK-8 and Transwell assays. **J** Expression of MYO18A in iCCA and pCCA was detected with IHC, and patients were categorized into low or high MYO18A subsets, Scale bar: 100 μm. **K** Patients with different expression patterns of Smad4 and MYO18A had distinct prognoses. n.s. represents not significant; *** represents $P < 0.001$, analyzed with one-way or two-way ANOVA (**H**, **I**) or log-rank test (**K**). Three independent experiments were performed.

for International Cancer Control (UICC), which further separated eCCA into pCCA and dCCA in 2007 [34]. The new classification was mainly based on their different anatomical locations and surgical procedures, but the biological and oncological differences between pCCA and dCCA are still obscure. Most studies still regarded pCCA and dCCA as the same histological type and did not treat them separately. In our NGS data, we showed for the first time that pCCA and dCCA had different GAs. Some genes, such as *AR1D1A, KMT2D*, and *CAMTA1*, had more frequent GA rates in dCCA, while the GA rates of some other genes, such as CTNNB1,

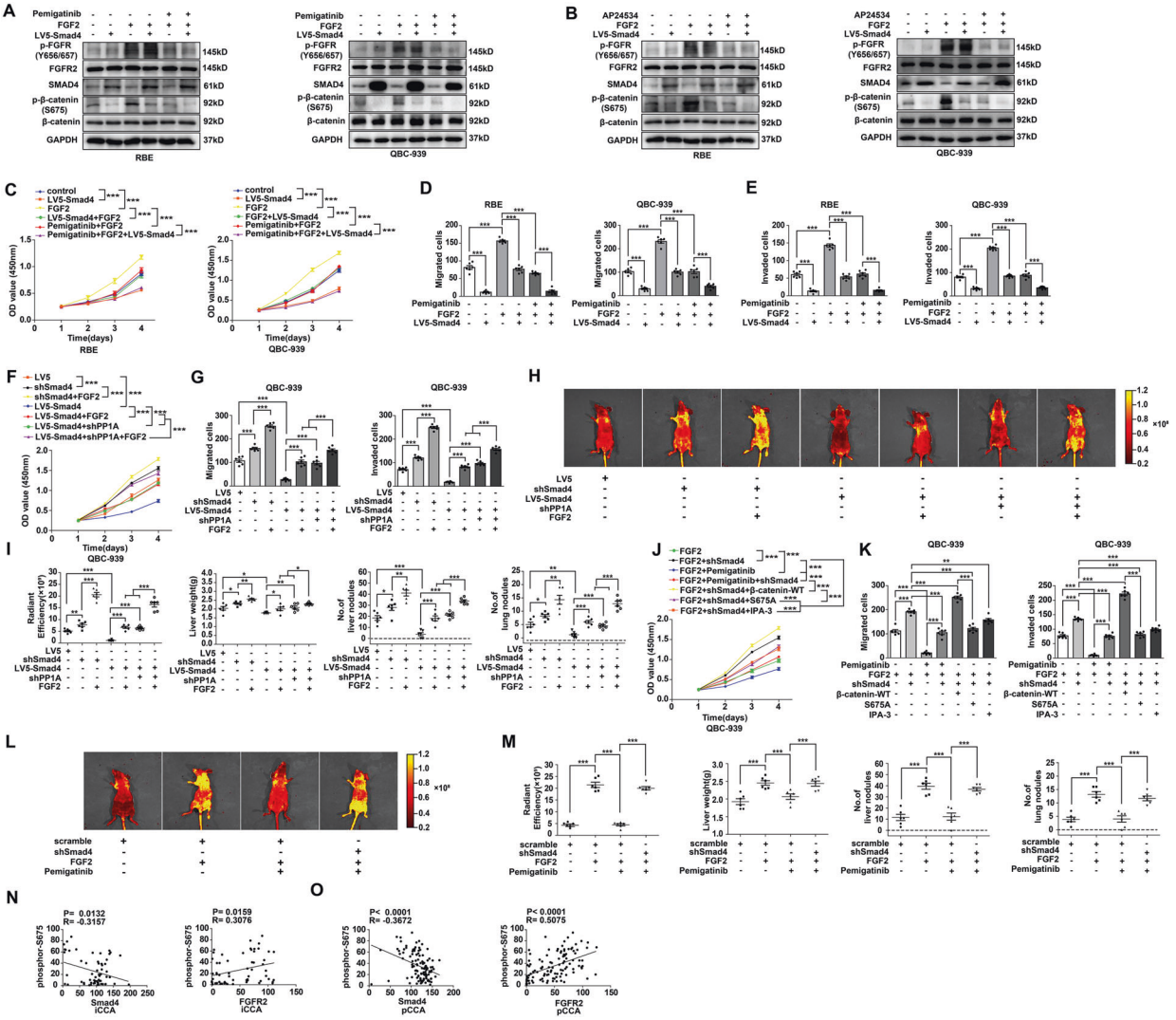

Fig. 6 Smad4 suppressed FGFR2-induced progression in CCA by inhibiting β-catenin phosphorylation. A, **B** After treatment with FGF2 (100 ng/ml, 10 min), Pemigatinib (10 nM, 8 h), or AP24534 (10 nM, 8 h), the phosphorylation of FGFR and β-catenin in RBE and QBC-939 cells was detected. **C**–**E** Smad4-overexpressing or Smad4-silenced RBE or QBC-939 cells were incubated in FGF2 and/or Pemigatinib. Cell proliferation (**C**), migration (**D**), and invasion (**E**) were detected. **F**, **G** QBC-939 cells were transfected with plasmids encoding shSmad4, Lv5-Smad4, or shPP1A and incubated with/without FGF2. Cell proliferation (**F**), migration and invasion (**G**) were detected. **H** Metastatic models were established by tail vein injection of Smad4-overexpressing or Smad4-silenced QBC-939 cells in which PP1A was simultaneously knocked down, FGF2 (100 mg/kg i.p.) were used to activate FGFR in vivo. The tumor metastases were monitored by a live imaging system. **I** The radiant efficiency of in vivo fluorescence, liver weight, and metastatic nodules in the liver and lungs in (**H**) were measured. **J**, **K** QBC-939 cells were transfected with plasmids encoding shSmad4, β-catenin-WT or β-catenin-S675A and incubated with/without Pemigatinib. Cell proliferation (**J**), migration, and invasion (**K**) were detected. **L** Metastatic models were established by tail vein injection of scramble cells or Smad4-silenced QBC-939 cells, in the presence of FGF2 (100 mg/kg i.p.) or Pemigatinib (10 mg/kg i.p.). **M** The radiant efficiency of in vivo fluorescence, liver weight, and metastatic nodules in the liver and lungs in (**L**) were measured. The correlations between Smad4 and β-catenin-S675 phosphorylation (**N**), between FGFR2 and β-catenin-S675 phosphorylation (**O**) in iCCA and pCCA were analyzed with the Pearson correlation test. *$P < 0.05$; **$P < 0.01$; ***$P < 0.001$, analyzed with one-way (**D**, **E**, **G**, **I**, **K**, **M**) or two-way ANOVA (**C**, **F**, **J**). Three independent experiments were performed.

were higher in pCCA. The TMB in pCCA and dCCA also showed a significant difference in our study. Though the GA rates of *SMAD4* in pCCA and dCCA were similar, but the prognostic value of Smad4 in dCCA was insignificant. These results support that pCCA and dCCA are distinct biological and histological CCA subtypes.

An important dilemma of CCA-targeted therapy is the scarcity of cohort studies with large sample sizes. The radical surgery rate of CCA is extremely low because of the anatomical difficulty of porta hepatis and the clinical signatures of CCA including rapid progression and severe invasion to lymph nodes, vessels and nerves. A low surgery rate results in the difficulty of obtaining specimens and establishing a patient cohort, which further limits advancements in CCA biomarker studies and the promotion of targeted therapy. In our study, our CCA cohort consisted of 261 patients, which was a relatively large sample size for CCAs. We showed that Smad4 was a prognostic biomarker in iCCA and pCCA and that the prognosis of patients with Smad4 and MYO18A coexpression was more favorable than that of those with expression of only Smad4/MYO18A. Our results suggested the importance of Smad4 and MYO18A detection in CCA patients, which could stratify high-risk patients to more precisely guide individualized treatments.

Serine and threonine phosphorylation account for 98.2% of all amino acid phosphorylation events, and the PP1 phosphatase

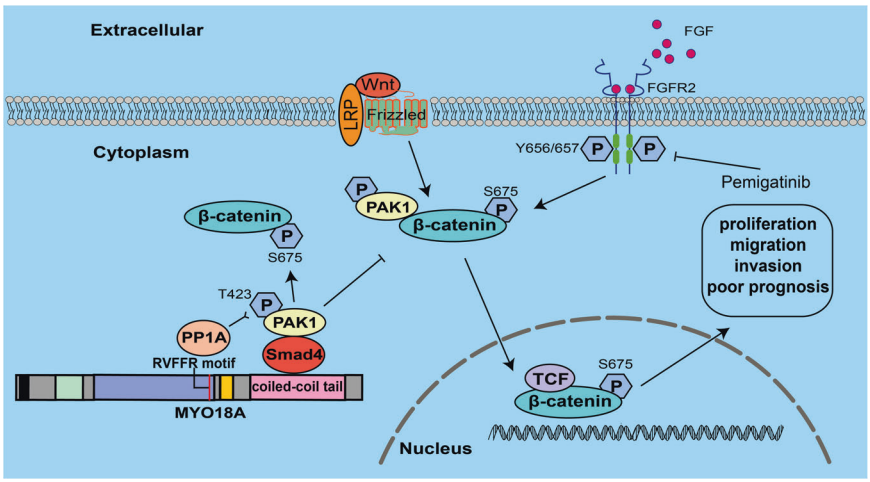

Fig. 7 Schematic depiction of the mechanism by which Smad4 suppresses β-catenin-S675 phosphorylation and FGF2-induced tumor progression. MYO18A interacts with PP1A via its RVFFR motif and binds Smad4 via its coiled coil tail domain. This MYO18A-PP1A-Smad4 complex recognizes and dephosphorylates phospho-PAK1-T423, which further decreases β-catenin-S675 phosphorylation and inhibits β-catenin intranuclear localization. Activation of FGFR also phosphorylates β-catenin-S675 and increases the intranuclear accumulation of β-catenin. The phosphorylation of β-catenin-S675 can facilitate β-catenin translocation into the nucleus and drive CCA progression. Smad4 suppresses CCA proliferation, migration and invasion, and high expression of Smad4 is associated with a favorable prognosis in CCA patients.

family, including PP1A, PP1B, PP1D and PP1G, catalyzes more than half of the dephosphorylation reactions of all phosphoserine/threonine residues in mammalian cells [35]. The amino acid sequences of mammalian PP1 isoforms are approximately 90% identical, and their substrate specificity and even catalytic activity are determined by PIPs [36]. For the first time, we identified MYO18A as a PIP for PP1A in the process of catalysis of phospho-PAK1-T423. Moreover, we identified the binding motif of MYO18A and revealed the necessity of that MYO18A constituted a complex with PP1A and Smad4 by RVFFR motif and CC domain. This finding is an important supplement to the PP1A catalysis mechanism, which expands the substrate diversity of PP1A and defines a new substrate recognition mechanism of PP1A.

Moreover, our results propose a new paradigm of Smad4-suppressing cancer progression. Smad4 forms a complex with MYO18A and PP1A and therefore suppresses the phosphorylation and intranuclear translocation of β-catenin in a TGF-β-independent manner. This synergistic effect of Smad4 and MYO18A facilitates the PP1A dephosphorylation towards phospho-PAK1-T423 and attenuates β-catenin-S645 phosphorylation, thus inhibits CCA progression and leads to favorable outcomes (Fig. 7). Considering the universality of both Smad4 deletion and Wnt/β-catenin activation in cancer, this new paradigm may provide a novel direction for studying the mechanisms of tumor progression and a new intervention target for clinical investigations, not only for CCA but also for most other tumor types. However, some other important issues should be solved in the future. For example, how Smad4 recognizes and interacts with PAK1 and how nuclear β-catenin leads to CCA progression are worthy of further investigations.

β-catenin is a key node in many signaling pathways in addition to Wnt signaling, and its various post-translational modifications determine its intracellular locations and functions [37]. In general, β-catenin can be phosphorylated by the destruction complex, which is composed of the scaffold protein Axin, adenomatous polyposis coli protein (APC), glycogen synthase kinase 3β (GSK3β) and casein kinase I isoform-α (CK1α), resulting in the ubiquitination and degradation of β-catenin. Wnt signaling activation inhibits β-catenin ubiquitination and facilitates β-catenin translocation into the nucleus to activate target genes. Previous reports stated that Smad4 was able to suppress Wnt/β-catenin signaling in both physiological and pathological processes [38–40], but the mechanism is still ambiguous. In colorectal cancer, the Smad4-BMP axis inhibits Wnt signaling by suppressing β-catenin expression [17]. However, our results showed that the phosphorylation and intracellular localization, instead of the expression, of β-catenin was regulated by Smad4 in CCA. The important oncogenic role of Wnt/β-catenin in CCA progression was demonstrated in our previous study [22, 41], so elaborating the underlying mechanism of how Smad4 modulates Wnt/β-catenin signaling is a pivotal issue in CCA progression. A previous study indicated that β-catenin-S675 can be phosphorylated by PAK1 [30]. Here, we expand the knowledge of β-catenin modification by demonstrating that Smad4 inhibits the phosphorylation of β-catenin-S675 by facilitating the interaction between PP1A and PAK1, which is the kinase of β-catenin-S675 in CCA. Our results unveil a new Smad4-mediated modification of β-catenin and suggest the oncogenic potency of β-catenin-S675 phosphorylation in CCA progression. Moreover, our results indicate promising direction of CCA-targeted drugs, since PAK1 has multiple preclinical inhibitors, and some of them are in clinical trials [42]. Targeting PAK1 or manipulating β-catenin phosphorylation may be a potential intervention for CCA-targeted therapy.

FGFR2 is one of the most well-known biomarkers of CCA, and its inhibitor Pemigatinib is currently the only FDA-approved targeted drug for CCA. β-catenin was previously reported to be activated and translocated into the nucleus in response to stimulation by growth factors such as FGF [33, 43], and Smad4 could be regulated by both FGF/MAPK and Wnt/GSK3 phosphorylation [33]. The crosstalk between Wnt/β-catenin signaling, FGF/FGFR signaling and Smad4 constitute a complex network. In this study, we showed that Smad4 overexpression enhanced the inhibitory effect of Pemigatinib and that Smad4 deletion significantly impaired the effect of Pemigatinib by modulating β-catenin phosphorylation. Pemigatinib is a newly developed drug for CCA, and little is known about its drug resistance. Our results suggest that Smad4 deletion could be a new attributor of Pemigatinib resistance, and that Smad4 detection could help select patients who may benefit from Pemigatinib treatment and guide individual treatment more precisely.

In conclusion, we investigated the genetic alteration, expression and clinical significance of Smad4 in CCA and identified Smad4 as a favorable prognostic biomarker. Based on the clinical analysis, we analyzed the correlations between Smad4 and β-catenin

phosphorylation and demonstrated that Smad4-mediated PAK1-T423 dephosphorylation, which was responsible for β-catenin-S675 phosphorylation and intranuclear localization in CCA. With LC–MS/MS and multiple biochemical techniques, we showed that PP1A was the phosphatase catalyzing phospho-PAK1-T423 and identified MYO18A as the PIP mediating the PP1A recognition toward PAK1. MYO18A interacts with PP1A via its RVFFR motif and interacts with Smad4 via its CC domain. This MYO18A-PP1A-Smad4 complex recognized and dephosphorylated phospho-PAK1-T423 in CCA. Moreover, Smad4 enhanced Pemigatinib efficiency, and Smad4 knockdown resulted in Pemigatinib resistance (Fig. 7). Our study provides additional evidence for more precise stratification and postoperative supervision of CCA patients and indicates that Smad4 and MYO18A detection could be applied to screen high-risk patients and may predict the effect of Pemigatinib. We delineate the oncogenic role of β-catenin-S675 phosphorylation in CCA, and more importantly, we propose a new paradigm in which Smad4 facilitates PAK1 dephosphorylation and modulates β-catenin-S675 phosphorylation by forming a complex with MYO18 and PP1A, which reveals an important mechanism of CCA progression and may provide new directions for CCA-targeted drug development.

DATA AVAILABILITY

No data was uploaded to the public database. All the data were available upon rational request.

REFERENCES

1. Rizvi S, Khan SA, Hallemeier CL, Kelley RK, Gores GJ. Cholangiocarcinoma—evolving concepts and therapeutic strategies. Nat Rev Clin Oncol. 2018;15:95–111.
2. Khan SA, Davidson BR, Goldin RD, Heaton N, Karani J, Pereira SP, et al. Guidelines for the diagnosis and treatment of cholangiocarcinoma: an update. Gut. 2012;61:1657–69.
3. Banales JM, Marin JJG, Lamarca A, Rodrigues PM, Khan SA, Roberts LR, et al. Cholangiocarcinoma 2020: the next horizon in mechanisms and management. Nat Rev Gastroenterol Hepatol. 2020;17:557–88.
4. Valle JW, Kelley RK, Nervi B, Oh DY, Zhu AX. Biliary tract cancer. Lancet. 2021;397:428–44.
5. Chen T, Li K, Liu Z, Liu J, Wang Y, Sun R, et al. WDR5 facilitates EMT and metastasis of CCA by increasing HIF-1alpha accumulation in Myc-dependent and independent pathways. Mol Ther. 2021;29:2134–50.
6. DeOliveira ML, Cunningham SC, Cameron JL, Kamangar F, Winter JM, Lillemoe KD, et al. Cholangiocarcinoma: thirty-one-year experience with 564 patients at a single institution. Ann Surg. 2007;245:755–62.
7. Li Z, Liu J, Chen T, Sun R, Liu Z, Qiu B, et al. HMGA1-TRIP13 axis promotes stemness and epithelial mesenchymal transition of perihilar cholangiocarcinoma in a positive feedback loop dependent on c-Myc. J Exp Clin Cancer Res. 2021;40:86.
8. Abou-Alfa GK, Sahai V, Hollebecque A, Vaccaro G, Melisi D, Al-Rajabi R, et al. Pemigatinib for previously treated, locally advanced or metastatic cholangiocarcinoma: a multicentre, open-label, phase 2 study. Lancet Oncol. 2020;21:671–84.
9. David CJ, Huang YH, Chen M, Su J, Zou Y, Bardeesy N, et al. TGF-beta tumor suppression through a lethal EMT. Cell. 2016;164:1015–30.
10. Kamisawa T, Wood LD, Itoi T, Takaori K. Pancreatic cancer. Lancet. 2016;388:73–85.
11. Inamoto S, Itatani Y, Yamamoto T, Minamiguchi S, Hirai H, Iwamoto M, et al. Loss of SMAD4 promotes colorectal cancer progression by accumulation of myeloid-derived suppressor cells through the CCL15-CCR1 chemokine axis. Clin Cancer Res. 2016;22:492–501.
12. Wang LH, Kim SH, Lee JH, Choi YL, Kim YC, Park TS, et al. Inactivation of SMAD4 tumor suppressor gene during gastric carcinoma progression. Clin Cancer Res. 2007;13:102–10.
13. Zhao M, Mishra L, Deng CX. The role of TGF-beta/SMAD4 signaling in cancer. Int J Biol Sci. 2018;14:111–23.
14. Wang F, Xia X, Yang C, Shen J, Mai J, Kim HC, et al. SMAD4 gene mutation renders pancreatic cancer resistance to radiotherapy through promotion of autophagy. Clin Cancer Res. 2018;24:3176–85.
15. Nakamura H, Arai Y, Totoki Y, Shirota T, Elzawahry A, Kato M, et al. Genomic spectra of biliary tract cancer. Nat Genet. 2015;47:1003–10.
16. Wardell CP, Fujita M, Yamada T, Simbolo M, Fassan M, Karlic R, et al. Genomic characterization of biliary tract cancers identifies driver genes and predisposing mutations. J Hepatol. 2018;68:959–69.
17. Freeman TJ, Smith JJ, Chen X, Washington MK, Roland JT, Means AL, et al. Smad4-mediated signaling inhibits intestinal neoplasia by inhibiting expression of beta-catenin. Gastroenterology. 2012;142:562–71.e2.
18. Voorneveld PW, Kodach LL, Jacobs RJ, van Noesel CJ, Peppelenbosch MP, Korkmaz KS, et al. The BMP pathway either enhances or inhibits the Wnt pathway depending on the SMAD4 and p53 status in CRC. Br J Cancer. 2015;112:122–30.
19. Zhi X, Lin L, Yang S, Bhuvaneshwar K, Wang H, Gusev Y, et al. betaII-Spectrin (SPTBN1) suppresses progression of hepatocellular carcinoma and Wnt signaling by regulation of Wnt inhibitor kallistatin. Hepatology. 2015;61:598–612.
20. Petit FG, Deng C, Jamin SP. Partial Mullerian Duct Retention in Smad4 Conditional Mutant Male Mice. Int J Biol Sci. 2016;12:667–76.
21. Moz S, Basso D, Bozzato D, Galozzi P, Navaglia F, Negm OH, et al. SMAD4 loss enables EGF, TGFbeta1 and S100A8/A9 induced activation of critical pathways to invasion in human pancreatic adenocarcinoma cells. Oncotarget. 2016;7:69927–44.
22. Liu Z, Sun R, Zhang X, Qiu B, Chen T, Li Z, et al. Transcription factor 7 promotes the progression of perihilar cholangiocarcinoma by inducing the transcription of c-Myc and FOS-like antigen 1. EBioMedicine. 2019;45:181–91.
23. Xu YF, Yang XQ, Lu XF, Guo S, Liu Y, Iqbal M, et al. Fibroblast growth factor receptor 4 promotes progression and correlates to poor prognosis in cholangiocarcinoma. Biochem Biophys Res Commun. 2014;446:54–60.
24. Sun R, Liu Z, Qiu B, Chen T, Li Z, Zhang X, et al. Annexin10 promotes extrahepatic cholangiocarcinoma metastasis by facilitating EMT via PLA2G4A/PGE2/STAT3 pathway. EBioMedicine. 2019;47:142–55.
25. Qiu B, Chen T, Sun R, Liu Z, Zhang X, Li Z, et al. Sprouty4 correlates with favorable prognosis in perihilar cholangiocarcinoma by blocking the FGFR-ERK signaling pathway and arresting the cell cycle. EBioMedicine. 2019;50:166–77.
26. Churi CR, Shroff R, Wang Y, Rashid A, Kang HC, Weatherly J, et al. Mutation profiling in cholangiocarcinoma: prognostic and therapeutic implications. PloS ONE. 2014;9:e115383.
27. Ong CK, Subimerb C, Pairojkul C, Wongkham S, Cutcutache I, Yu W, et al. Exome sequencing of liver fluke-associated cholangiocarcinoma. Nat Genet. 2012;44:690–3.
28. Montal R, Sia D, Montironi C, Leow WQ, Esteban-Fabro R, Pinyol R, et al. Molecular classification and therapeutic targets in extrahepatic cholangiocarcinoma. J Hepatol. 2020;73:315–27.
29. Sia D, Hoshida Y, Villanueva A, Roayaie S, Ferrer J, Tabak B, et al. Integrative molecular analysis of intrahepatic cholangiocarcinoma reveals 2 classes that have different outcomes. Gastroenterology. 2013;144:829–40.
30. Spirli C, Locatelli L, Morell CM, Fiorotto R, Morton SD, Cadamuro M, et al. Protein kinase A-dependent pSer(675) -beta-catenin, a novel signaling defect in a mouse model of congenital hepatic fibrosis. Hepatology. 2013;58:1713–23.
31. Barrios-Rodiles M, Brown KR, Ozdamar B, Bose R, Liu Z, Donovan RS, et al. High-throughput mapping of a dynamic signaling network in mammalian cells. Science. 2005;307:1621–5.
32. Bollen M, Peti W, Ragusa MJ, Beullens M. The extended PP1 toolkit: designed to create specificity. Trends Biochem Sci. 2010;35:450–8.
33. Paek H, Hwang JY, Zukin RS, Hebert JM. beta-Catenin-dependent FGF signaling sustains cell survival in the anterior embryonic head by countering Smad4. Dev Cell. 2011;20:689–99.
34. Edge SB, Compton CC. The American Joint Committee on Cancer: the 7th edition of the AJCC cancer staging manual and the future of TNM. Ann Surg Oncol. 2010;17:1471–4.
35. Olsen JV, Blagoev B, Gnad F, Macek B, Kumar C, Mortensen P, et al. Global, in vivo, and site-specific phosphorylation dynamics in signaling networks. Cell. 2006;127:635–48.
36. Ferreira M, Beullens M, Bollen M, Van, Eynde A. Functions and therapeutic potential of protein phosphatase 1: insights from mouse genetics. Biochimica Biophys Acta Mol Cell Res. 2019;1866:16–30.
37. Stamos JL, Weis WI. The beta-catenin destruction complex. Cold Spring Harb Perspect Biol. 2013;5:a007898.
38. Li J, Huang X, Xu X, Mayo J, Bringas P Jr., Jiang R, et al. SMAD4-mediated WNT signaling controls the fate of cranial neural crest cells during tooth morphogenesis. Development. 2011;138:1977–89.
39. Jia L, Lee HS, Wu CF, Kundu J, Park SG, Kim RN, et al. SMAD4 suppresses AURKA-induced metastatic phenotypes via degradation of AURKA in a TGFbeta-independent manner. Mol Cancer Res. 2014;12:1779–95.
40. Salazar VS, Zarkadis N, Huang L, Watkins M, Kading J, Bonar S, et al. Postnatal ablation of osteoblast Smad4 enhances proliferative responses to canonical Wnt signaling through interactions with beta-catenin. J Cell Sci. 2013;126:5598–609.

41. Boulter L, Guest RV, Kendall TJ, Wilson DH, Wojtacha D, Robson AJ, et al. WNT signaling drives cholangiocarcinoma growth and can be pharmacologically inhibited. J Clin Investig. 2015;125:1269–85.
42. Semenova G, Chernoff J. Targeting PAK1. Biochemical Soc Trans. 2017;45:79–88.
43. Demagny H, Araki T, De Robertis EM. The tumor suppressor Smad4/DPC4 is regulated by phosphorylations that integrate FGF, Wnt, and TGF-beta signaling. Cell Rep. 2014;9:688–700.

AUTHOR CONTRIBUTIONS

JL, GR, KL, ZL, YW, TC, WM, XL, AS, and WZ performed experiments. XY reviewed pathology. BX, JC, SG, CP, and TZ collected the specimens and followed up the patients. ZZ collected the specimens and supervised the study. YX designed the study and wrote the paper.

FUNDING

Our study was supported by Shandong University Multidisciplinary Research and Innovation Team of Young Scholars (Grant No. 2020QNQT002), National Natural Science Foundation of China (Grant No. 82072676, 82172791), China Postdoctoral Science Foundation (Grant No. 2020M682190, 2020M682195), Clinical Research Foundation of Shandong University (Grant No. 2020SDUCRCA018), Natural Science Foundation of Shandong Province (ZR2019MH008), Jinan City Science and Technology Development Program (Grant No. 201805017, 201805013), Clinical Research Innovation Fund Project (CXPJJH11800001–2018240), Hengrui Hepatobiliary and Pancreatic Foundation (Grant No.Y-2017-144), Key Research and Development Program of Shandong Province (Grant No. 2019GSF108254), Beijing Medical Award Foundation (YXJL-2020-0785-0967, YXJL-2020-0785-0968).

COMPETING INTERESTS

The authors declare no competing interests.

ETHICS APPROVAL

All the patients provided their consents for specimen obtainment and data analysis. The study protocol were approved and supervised by the Ethics Committee of Qilu Hospital of Shandong University.

ADDITIONAL INFORMATION

Supplementary information The online version contains supplementary material available at https://doi.org/10.1038/s41418-021-00897-7.

Correspondence and requests for materials should be addressed to Zongli Zhang or Yunfei Xu.